

# SMALL-SIGNAL ANALYSIS AND CONTROL DESIGN OF ISOLATED POWER SUPPLIES WITH OPTOCOUPLER FEEDBACK

Yuri Panov and Milan Jovanović

Power Electronics Laboratory  
Delta Products Corporation  
P.O. Box 12173, 5101 Davis Drive  
Research Triangle Park, NC 27709, USA

**Abstract** - Optocouplers are widely used in isolated power supplies to transfer the feedback signal from the secondary to the primary side. In many power supplies, the feedback amplifier is supplied from the output voltage that creates additional feedback path which should be accounted in the control design. The paper compares two possible loop gains corresponding to breaking the feedback loop at different locations. These loop gains are analyzed and are shown to have an unequal value for the design. Dynamic limitations of the TL431 shunt regulator and the optocoupler are discussed. Practical guidelines for the error amplifier design and a design example are presented.

## I. INTRODUCTION

Generally, offline and telecom power supplies require the galvanic isolation between a relatively high input voltage and low output voltages. The most widely used devices to transfer signals across the isolation boundary are pulse transformers and optocouplers. The typical isolated power supply with the primary-side PWM control is shown in Fig. 1. The feedback signal is transferred from the secondary to the primary side through the optocoupler OC1. The feedback circuit shown in Fig.1 is very popular in low-power / low-cost power supplies which usually do not have the standby converter to supply the TL431 shunt regulator but use output voltage  $V_O$  for this purpose. It is well known [1-7] that by supplying the TL431 from the output voltage an additional feedback path is introduced. Therefore, in the control circuit in Fig. 1 two loop gains which correspond to breaking the loop at locations A and B can be considered. The existence of two loops immediately raises the question which loop gain should be analyzed and measured in order to meet the power supply stability and dynamic response specifications. From the general control theory, each loop gain of the entire control system yields the same characteristic polynomial and, therefore, reveals the system stability. However, depending on the chosen loop gain, error amplifier (EA) design is different which leads to different stability margins and different dynamic performance. So far, these issues have not been addressed in the literature.

The purpose of the paper is to present comparative analysis of the loop gains corresponding to points A and B and to provide design guidelines to power supply engineers. Section II of the paper provides general loop gain analysis and interpretation. Section III presents the comparative analysis of loop gains  $T_A$  and  $T_B$  for the power supplies with the voltage-mode and the current-mode controls. Section III also discusses EA design limitations of the TL431 shunt regulator and of the optocoupler circuit. Sections

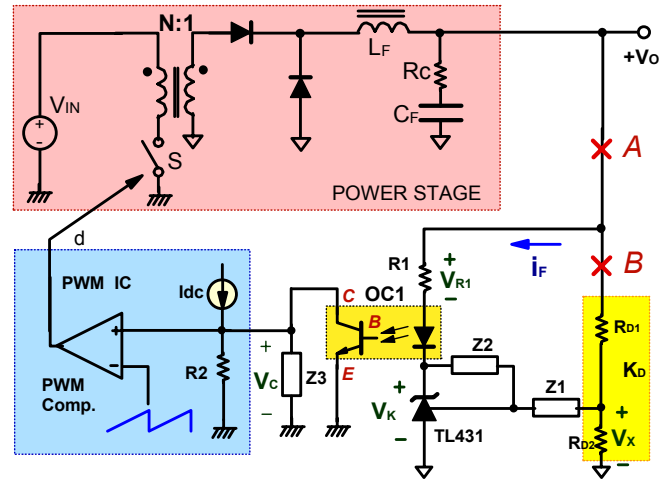


Fig. 1. Simplified circuit diagram of isolated power supply with optocoupler feedback.

IV and V present the design example and experimental results, respectively, whereas Section VI summarizes the paper.

## II. LOOP GAIN ANALYSIS AND INTERPRETATION

### A. Loop Gain $T_A$

The small-signal block diagram corresponding to breaking the loop at point A is shown in Fig. 2. Figure 2 contains following blocks:

$K_D$  – output voltage divider gain,

$G_{EA} = -\hat{V}_K / \hat{V}_X$  - error amplifier transfer function,

$A_{OC} = \hat{V}_C / \hat{V}_{R1}$  - optocoupler circuit gain,

$G_{VC} = \hat{V}_O / \hat{V}_C$  - control-to-output transfer function,

$G_{VV(OL)} = \hat{V}_O / \hat{V}_{IN}$  - open-loop audio susceptibility,

$Z_{O(OL)} = \hat{V}_O / \hat{i}_O$  - open-loop output impedance.

At point A in Fig. 2, the feedback signal is confined to a single path. Loop gain  $T_A$ , corresponding to breaking the loop at point A is derived as:

$$T_A = A_{OC} \cdot G_{VC} \cdot (1 + K_D \cdot G_{EA}) \quad (1)$$

The plant transfer function that provides the basis for the EA design is defined as

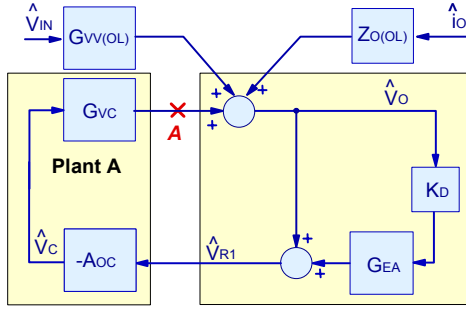


Fig. 2. Small-signal block diagram corresponding to breaking the loop at point A.

$$\mathbf{G}_{PL(A)} = A_{OC} \cdot \mathbf{G}_{VC} \cdot \quad (2)$$

It should be noted that the EA is not connected in series with the plant and zeroes of  $\mathbf{G}_{EA}$  generally do not translate into the same zeroes of the loop gain  $T_A$ . However, in many cases,  $K_D \cdot \mathbf{G}_{EA} \gg 1$  within the loop bandwidth and loop gain  $T_A$  can be written as

$$T_A \approx \mathbf{G}_{PL(A)} \cdot K_D \cdot \mathbf{G}_{EA} \cdot \quad (3)$$

For loop gain  $T_A$  given in (3), the EA design procedure does not differ from that for the implementation where the optocoupler is supplied from the fixed voltage. If condition  $K_D \cdot \mathbf{G}_{EA} \gg 1$  is not satisfied within the loop bandwidth, the relationship between the zeroes of terms  $K_D \cdot \mathbf{G}_{EA}$  and  $[1 + K_D \cdot \mathbf{G}_{EA}]$  can be very complex, particularly, when the EA transfer function has more than two poles. To simplify the EA design in this case, it is recommended to keep the order of the EA transfer function not higher than two, but to add necessary poles and zeroes by connecting compensation network  $Z_3$  on the primary side, as shown in Fig. 1. There is one more reason to connect compensation network  $Z_3$  on the primary side. Term  $[1 + K_D \cdot \mathbf{G}_{EA}]$  in (1) has the slope of 0 dB/dec at high frequencies. To attenuate the switching noise at high frequencies, it is desirable to add the primary-side pole at the crossover frequency of term  $[1 + K_D \cdot \mathbf{G}_{EA}]$ .

It is important to find the relationship between loop gain  $T_A$  and the converter frequency-domain response to line and load variations. To simplify the analysis, it is assumed that the converter operates with the voltage-mode control. The closed loop audio susceptibility  $\mathbf{G}_{VV(CL)}$  and output impedance  $\mathbf{Z}_{O(CL)}$  are derived from the block diagram in Fig. 2 as

$$\mathbf{G}_{VV(CL)} = \frac{\mathbf{G}_{VV(OL)}}{1 + T_A} \quad \text{and} \quad \mathbf{Z}_{O(CL)} = \frac{\mathbf{Z}_{O(OL)}}{1 + T_A} \cdot \quad (4)$$

Relationships (4) are straightforward imply that it is desirable to maximize loop gain  $T_A$  in order to achieve the best rejection of the line and load disturbances.

### B. Loop Gain $T_B$

The small-signal block diagram corresponding to breaking the loop at point B is shown in Fig. 3. After opening the loop at point B, the feedback signal propagates through resistor  $R_1$  and affects LED current  $i_F$  in Fig. 1. Observation of the block diagram in Fig. 3 shows that after breaking the loop at location B the inner control loop still exists with the gain of

$$T_{INNER} = A_{OC} \cdot \mathbf{G}_{VC} \cdot \quad (5)$$

Loop gain  $T_B$ , corresponding to breaking at point B in Fig. 3, is derived as

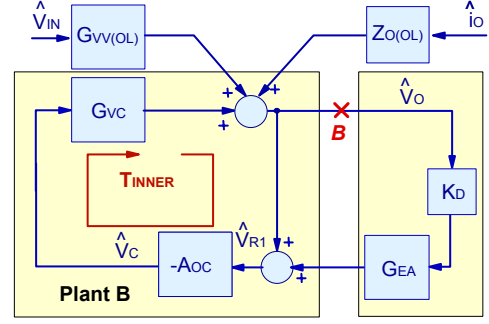


Fig. 3. Small-signal block diagram corresponding to breaking the loop at point B.

$$T_B = K_D \cdot \mathbf{G}_{EA} \cdot \frac{A_{OC} \cdot \mathbf{G}_{VC}}{1 + A_{OC} \cdot \mathbf{G}_{VC}} = K_D \cdot \mathbf{G}_{EA} \cdot \frac{T_{INNER}}{1 + T_{INNER}} \cdot \quad (6)$$

Generally, since loop B contains the inner feedback loop, the design of loop gain  $T_B$  is a two-step procedure. Namely, prior to loop gain  $T_B$  analysis,  $T_{INNER}$  gain must be examined for stability. The inner loop gain is relatively low because it does not contain the high-gain EA and its stability rarely becomes a practical problem. It should be noted that  $T_{INNER}$  can be compensated by connecting network  $Z_3$  on the primary side, as shown in Fig. 1, so that the design of loop gain  $T_B$  can be further optimized. The analysis and implementation of the inner loop compensation was presented in [8] in the context of the magamp control. In fact, the control of the isolated power supply with optocoupler supplied from the output voltage is similar to the magamp control where the magamp reset circuit is supplied from the output voltage [8, 9].

Equations (1), (5) and (6) are used to derive the relationship between  $T_A$  and  $T_B$ :

$$T_A = T_{INNER} + (1 + T_{INNER}) \cdot T_B \cdot \quad (7)$$

The last equation indicates that there is no unique relationship between  $T_A$  and  $T_B$ , unless  $T_{INNER}$  is known.

The plant transfer function that provides the basis for the EA design is defined as

$$\mathbf{G}_{PL(B)} = \frac{T_{INNER}}{1 + T_{INNER}} = \frac{A_{OC} \cdot \mathbf{G}_{VC}}{1 + A_{OC} \cdot \mathbf{G}_{VC}} = \frac{\mathbf{G}_{PL(A)}}{1 + \mathbf{G}_{PL(A)}} \cdot \quad (8)$$

Comparison of (2) and (8) reveals that the poles of plant transfer function  $\mathbf{G}_{PL(B)}$  are different from those of plant transfer function  $\mathbf{G}_{PL(A)}$ . Namely, at low frequencies, where  $T_{INNER} \gg 1$ , transfer function  $\mathbf{G}_{PL(B)} \approx 1$ . At high frequencies, where  $T_{INNER} \ll 1$ , transfer function  $\mathbf{G}_{PL(B)} \approx \mathbf{G}_{PL(A)}$ . The poles of  $\mathbf{G}_{PL(B)}$  are actually shifted to higher frequencies with respect to those of  $\mathbf{G}_{PL(A)}$  [8, 9]. Hence, the compensator poles and zeroes are selected differently depending on which loop gain,  $T_A$  or  $T_B$ , is used for the design.

Loop gain  $T_B$  can be written as

$$T_B = \mathbf{G}_{PL(B)} \cdot K_D \cdot \mathbf{G}_{EA} \cdot \quad (9)$$

From the block diagram in Fig. 3, the relationship between loop gain  $T_B$  and closed-loop audio susceptibility  $\mathbf{G}_{VV(CL)}$  and output impedance  $\mathbf{Z}_{O(CL)}$  of the converter with the voltage-mode control is

$$\mathbf{G}_{VV(CL)} = \frac{\mathbf{G}_{VV(OL)}}{1 + T_B} = \frac{\mathbf{G}_{VV(B)}}{1 + T_B}, \quad \text{and}$$

$$Z_{O(CL)} = \frac{Z_{O(OL)} / (1 + T_{INNER})}{1 + T_B} = \frac{Z_{CL(B)}}{1 + T_B}, \quad (10)$$

$$\text{where } G_{VV(B)} = \frac{G_{VV(OL)}}{1 + T_{INNER}} \text{ and } Z_{CL(B)} = \frac{Z_{O(OL)}}{1 + T_{INNER}}. \quad (11)$$

It should be noted that transfer functions  $G_{VV(B)}$  and  $Z_{CL(B)}$  given in (11) represent the audio susceptibility and output impedance of the converter with only the inner loop closed. Equations (10) and (11) indicate that for optimal rejection of line and load disturbances loop gain  $T_B$  as well as loop gain  $T_{INNER}$  should be maximized. Loop gain  $T_{INNER}$  can be maximized by compensating optocoupler circuit gain  $A_{OC}$ , whereas loop gain  $T_B$  can be optimized by compensating EA gain  $G_{EA}$ . However, placement of  $A_{OC}$  poles and zeroes at desired locations is not straightforward because their frequencies are dependent on the optocoupler circuit small-signal parameters, as it will be shown in Section III. Moreover, loop gain  $T_{INNER}$  affects plant transfer function  $G_{PL(B)}$  which is the basis for the EA design. Therefore, the design procedure for optimization of the audiosusceptibility and output impedance based on breaking the loop gain at point B is more complex than in the case of the design based on loop gain  $T_A$ . The purpose of the next Section is to compare EA designs based on loop gains  $T_A$  and  $T_B$ .

### III. ERROR AMPLIFIER DESIGN CONSIDERATIONS

#### A. Power Supplies with Voltage-Mode Control

Control-to-output transfer function  $G_{VC}$  of the forward converter in Fig. 1 in the case of the voltage-mode control becomes

$$G_{VC} = F_M \cdot G_{VD}, \quad (12)$$

where  $F_M$  is the gain of the pulse-width modulator (PWM) that is shown inside the control IC in Fig. 1.

Then, plant transfer functions  $G_{PL(A)}$  and  $G_{PL(B)}$  of the converter operating in CCM can be written as

$$G_{PL(A)} = A_{OC} \cdot F_M \cdot G_{VD}, \quad (13)$$

$$G_{PL(B)} = \frac{G_{PL(A)}}{1 + G_{PL(A)}}, \quad (14)$$

$$\text{where } G_{VD} = \frac{V_{IN}}{N} \cdot \frac{1 + s/\omega_{ZC}}{1 + s/(\omega_0 \cdot Q) + s^2/\omega_0^2}, \quad (15)$$

$$\omega_0 = \frac{1}{\sqrt{L_F \cdot C_F}}, \quad Q = \frac{\sqrt{L_F \cdot C_F}}{L_F/R_L + R_C \cdot C_F}, \quad \omega_{ZC} = \frac{1}{R_C \cdot C_F} \text{ and } R_L$$

is the load resistance. Equations (13) and (15) indicate that transfer function  $G_{PL(A)}$  has a pair of complex-conjugate poles near resonant frequency  $f_{0A} = \omega_0 / (2 \cdot \pi)$ .

To achieve stability and high dynamic performance, the EA transfer function for the voltage-mode control has two zeroes and three poles:

$$G_{EA} = \frac{\omega_i \cdot [1 + s/\omega_{Z1}] \cdot [1 + s/\omega_{Z2}]}{s \cdot [1 + s/\omega_{P1}] \cdot [1 + s/\omega_{P2}]}. \quad (16)$$

Asymptotic Bode plots of the plant and EA transfer functions, as well as of loop gain  $T_A$ , are shown in Fig. 4 for the

compensation design based on loop gain  $T_A$ . Compensation zero  $f_{Z1}$  is placed at plant A resonant frequency  $f_{0A}$  and zero  $f_{Z2}$  is placed between  $f_{0A}$  and expected loop crossover frequency  $f_c$ . Compensation pole  $f_{P1}$  is placed at the ESR zero frequency, and pole  $f_{P2}$  is placed between  $f_{P1}$  and the switching frequency. Both loop gains  $T_A$  and  $T_B$  have same crossover frequency  $f_c$  and expected to have similar stability margins. Since the loop gains cross 0 dB axis with the  $-1$  slope, the phase margin up to  $90^\circ$  is anticipated.

When the EA design is based on loop gain  $T_B$ , the corresponding asymptotic Bode plots are shown in Fig. 5. Plant B has the resonant frequency  $f_{0B} \approx f_{0A} \cdot \sqrt{1 + G_{PL(A)}(0)}$  [9].

Compensator zero  $f_{Z1}$  is placed between  $f_{0A}$  and  $f_{0B}$ , whereas compensator zero  $f_{Z2}$  is placed around  $f_{0B}$ . Observation of loop gain  $T_A$  in Fig. 5 indicates the conditional stability since the phase can go down to  $-270^\circ$  within the loop bandwidth. The conditionally stable loop becomes unstable when the loop gain is reduced. It is particularly unacceptable in the case of the optocoupler feedback since the optocoupler CTR varies significantly with temperature variations and with aging. It should be noted that loop gain  $T_B$  shows no sign of the conditional stability since it does not reveal the low-frequency dynamics of the power supply. The conditional stability can be avoided if compensator zero  $f_{Z1}$  is placed below resonant frequency  $f_{0A}$  of plant A. Then, loop gain  $T_A$  has  $-2$  slope in the frequency range between  $f_{0A}$  and  $f_{0B}$ , and  $T_A$  phase characteristic does not go below  $-180^\circ$ .

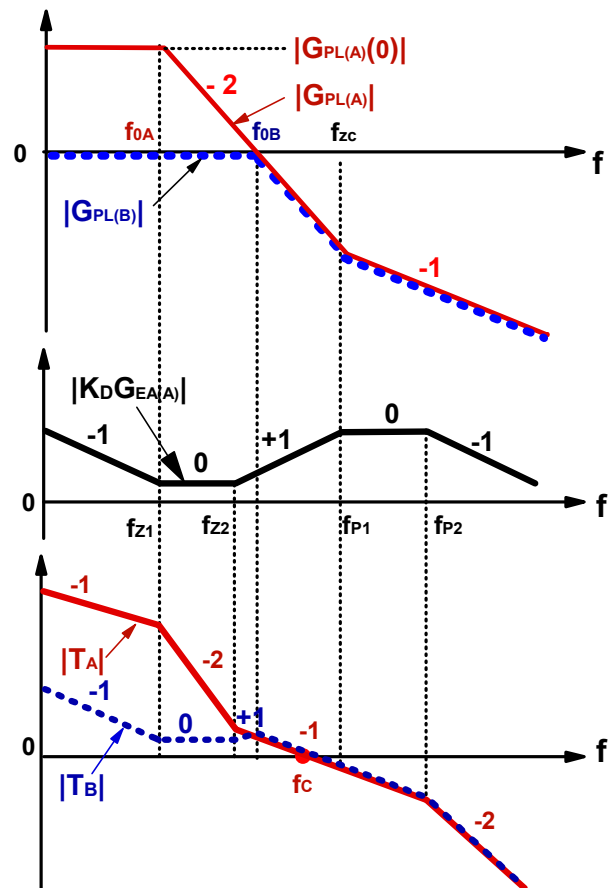


Fig. 4. EA design based on loop gain  $T_A$  for voltage-mode control.

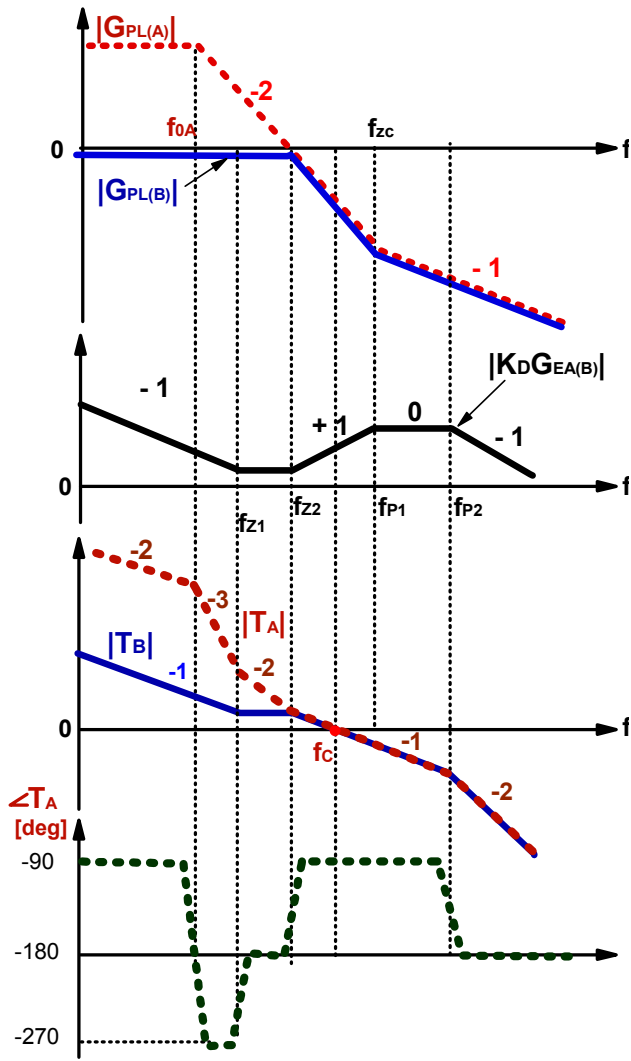


Fig. 5. EA design based on loop gain  $T_B$  for voltage-mode control.

### B. Power Supplies with Current-Mode Control

In the case of the current-mode control, the ramp signal for the PWM in Fig. 1 is derived by measuring the inductor  $L_F$  current. It should be noted that in real power supplies the measurement of the inductor current is replaced with the measurement of the primary switch current. Simplified control-to-output transfer function of the forward converter with the current-mode control is given by [10]

$$G_{PL(A)} = A_{OC} \cdot G_{VC} = A_{OC} \cdot \frac{R_L}{R_S} \cdot \frac{1+s/\omega_{ZC}}{1+s/\omega_{PA}}, \quad (17)$$

where frequencies of poles and zeroes are  $\omega_{ZC} = 1/(R_C \cdot C_F)$  and  $\omega_{PA} = 1/[(R_L + R_C) \cdot C_F]$ , and  $R_S$  is the current-sensing gain.

To explain the EA design, asymptotic Bode plots of the converter transfer functions are employed. The asymptotic Bode plots of the plant transfer functions  $G_{PL(A)}$  and  $G_{PL(B)}$  are shown in Fig. 6. Plant B has higher pole frequency  $f_{0B}$  than that of plant A which is governed by equation:

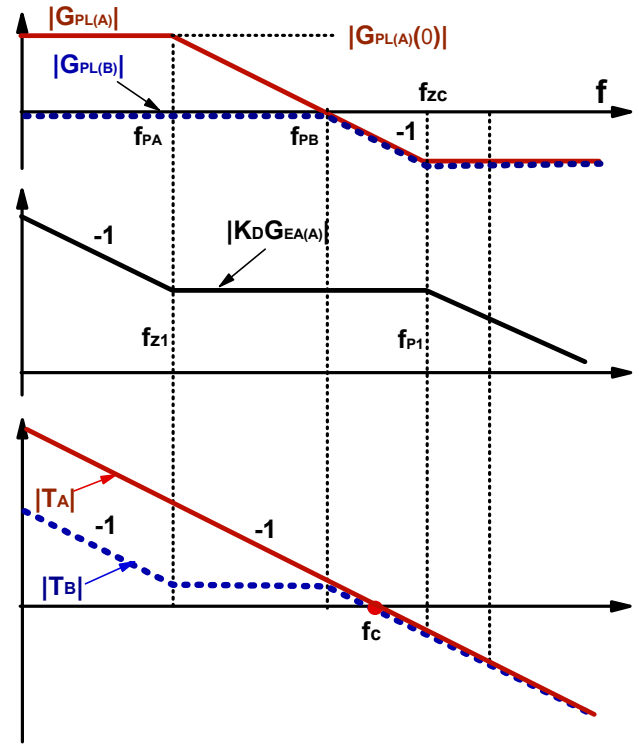


Fig. 6. EA design based on loop gain  $T_A$  for current-mode control.

$$f_{PB} \approx f_{PA} \cdot G_{PL(A)}(0). \quad (18)$$

As can be seen in Fig. 6,  $G_{PL(B)}$  magnitude stays close to unity in the frequency range below  $f_{PB}$ . Therefore, the transfer function of plant B does not reveal the low-frequency dynamic characteristics of the power stage. Fig. 6 also shows the asymptotic Bode plot of the compensation network for plant A with one zero and two poles

$$1 + K_D \cdot G_{EA} \approx K_D \cdot G_{EA} = \frac{\omega_i \cdot [1 + s/\omega_{Z1}]}{s \cdot [1 + s/\omega_{P1}]}, \quad (19)$$

which is typically used in converters with the current-mode control. The compensation zero  $f_{Z1} = \omega_{Z1}/(2\pi)$  is placed at pole  $f_{PA}$  frequency, and compensation pole  $f_{P1} = \omega_{P1}/(2\pi)$  is placed at zero  $f_{ZC}$  frequency. The resulting asymptotic Bode plots of loop gains  $T_A$  and  $T_B$  in Fig. 6 have same crossover frequency  $f_c$  and expected to have similar ample stability phase margins.

When the error amplifier design is based on loop gain  $T_B$ , the corresponding asymptotic Bode plots are shown in Fig. 7. Compensation zero  $f_{Z1}$  and pole  $f_{P1}$  are placed to coincide with pole  $f_{PB}$  and zero  $f_{ZC}$ , respectively. As Fig. 7 demonstrates, crossover frequencies and the predicted phase margins are essentially the same for loop gains  $T_A$  and  $T_B$ . Since the loop gains cross the 0 dB axis with the  $-1$  slope, the phase margin is expected to be close to  $90^\circ$ .

### C. TL431 Frequency Response Limitations

Subsections A and B were presented assuming that EA transfer function  $G_{EA}$  is completely determined by compensation networks  $Z_1$  and  $Z_2$ , namely,

$$G_{EA} = Z_2/Z_1. \quad (20)$$

This assumption is valid only when the EA has the infinite gain

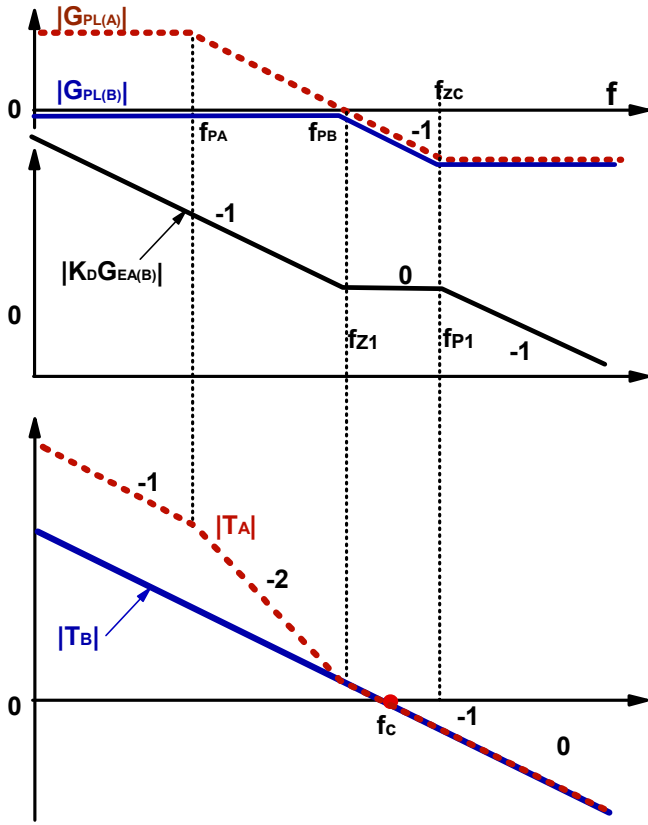


Fig. 7. EA design based on loop gain  $T_B$  for current-mode control.

in the frequency range of interest. If the TL431 finite gain-bandwidth product is accounted, the EA transfer function can be derived as:

$$G_{EA} = \frac{Z_2}{Z_1 + (Z_1 + Z_2)/B_{TL431}}, \quad (21)$$

where  $B_{TL431}(s)$  is the TL431 open-loop gain. If the  $B_{TL431}$  characteristic were well defined, the last equation would provide for an accurate EA design. Unfortunately, the information about the TL431 open-loop frequency response, available from the manufacturer data sheets, is very sketchy and insufficient for the accurate EA design. In addition, the TL431 frequency response strongly depends on the regulator bias cathode current and values of the components connected to its output, namely,  $R_1$  and  $Z_2$ . Nevertheless, based on the authors' practical experience, several practical observations can be made.

First, for EA transfer function  $G_{EA}$  to be completely determined by (20), relationship

$$G_{EA} \ll B_{TL431} - 1 \quad (22)$$

must be observed. Inequality (22) is practically observed if its left side is by 34-40 dB less than its right side. If (22) is violated, but still  $G_{EA} < B_{TL431} - 1$ , then (21) can be used with the typical values of 50-60 dB dc gain and 1 MHz bandwidth. The TL431 certainly cannot implement the EA transfer function whose gain is above the shunt regulator open loop gain.

Second, as in the case of an operational amplifier, the large capacitance connected to the TL431 output severely limits the regulator bandwidth. Therefore, compensation network  $Z_2$

should be implemented with the minimum capacitance amount. Namely, the value of the capacitor between the TL431 cathode and reference pins should not exceed several hundred pF.

#### D. Optocoupler Circuit Small-Signal Model

The dynamic model of the isolated power supply is incomplete without considering the small-signal characteristics of the optocoupler. The optocoupler small-signal model [11], corresponding to the circuit in Fig. 1, is shown in Fig. 8. The circuit in Fig. 8 contains the bipolar transistor hybrid model in the common-emitter configuration with following parameters:  $h_{ie}$  – input resistance with shorted output,  $h_{oe}$  – output conductance with open input,  $h_{fe}$  – forward amplification gain. The phototransistor model in Fig. 8 also includes collector-base junction capacitance  $C_{CB}$  and two dependent current sources  $\hat{i}_p = \hat{i}_F \cdot CTR/h_{fe}$  and  $h_{fe} \cdot \hat{i}_B$ . Since the collector-base junction in phototransistors is used as a light detector, its area is relatively large. As a result, phototransistors have high capacitance  $C_{CB}$  that limits their bandwidth. The typical values of the optocoupler parameters used in the power supplies are  $C_{CB} = 15$  pF and  $h_{FE} = 350$ . Using the diagram in Fig. 8 and assuming  $\hat{V}_{BE} \ll \hat{V}_{CE}$ ,  $1/h_{OE} \gg R_2 \parallel Z_3$ , the optocoupler circuit transfer function is derived:

$$A_{OC} = \frac{CTR}{R_1} \cdot \frac{1}{1/(R_2 \parallel Z_3) + s \cdot C_{CB} \cdot h_{FE}}. \quad (23)$$

When network  $Z_3$  consists of single capacitor  $C_2$ , equation (23) is simplified to:

$$A_{OC} = CTR \cdot \frac{R_2}{R_1} \cdot \frac{1}{1 + s/\omega_{OC}}, \quad (24)$$

where  $\omega_{OC} = 1/[R_2 \cdot (C_2 + h_{FE} \cdot C_{CB})]$ . It should be noted that the maximum value of pole frequency  $\omega_{OC}$  is limited by the phototransistor parameters  $C_{CB}$  and  $h_{FE}$ . For example, for  $R_2 = 1$  k $\Omega$  the frequency of this pole is below 30 kHz.

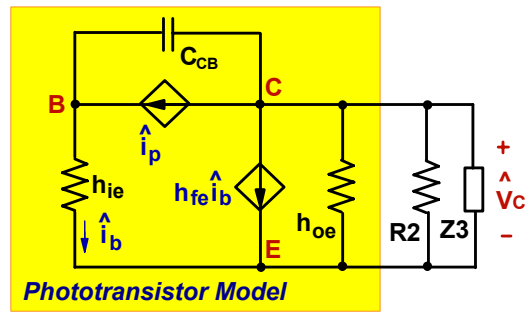


Fig. 8. Small-signal model of the optocoupler circuit.

#### IV. DESIGN EXAMPLE

This section considers the 380-V/5-V, 20-A, 100-kHz forward power supply, whose simplified schematic is shown in Fig. 1. Transformer with turns ratio  $N$  of 20:1 is assumed. The output filter inductor value is  $L_F = 10$   $\mu$ H, whereas output capacitance consists of two 3300- $\mu$ F aluminum capacitors with 18-m $\Omega$  ESR each. The design example also assumes  $F_M = 1$   $V^{-1}$

and the optocoupler circuit values of  $CTR = 100\%$  and  $R_1 = R_2 = 1 \text{ k}\Omega$ .

### A. Power Supply with Voltage Mode Control

The Bode plots of plant transfer functions  $G_{PL(A)}$  and  $G_{PL(B)}$  of the power supply with the voltage-mode control are shown in Fig. 9. The plant transfer functions in Fig. 9 are different at low frequencies where  $A_{OC} \cdot G_{VC} \gg 1$ . Actually, due to the inner loop influence, the loop gain  $T_B$  does not reveal the control loop dynamics at low frequencies where its value is close to unity. Also between resonant frequencies  $f_{0A} = 0.6 \text{ kHz}$  and  $f_{0B} = 2.8 \text{ kHz}$ , the phase lag of loop gain  $T_A$  is considerably higher than that of loop gain  $T_B$ . The plots in Fig. 9 indicate that it is much easier to design the EA for plant B than for plant A. The next step is to compare EA designs based on loop gains  $G_{PL(A)}$  and  $G_{PL(B)}$ .

Error Amplifier Design Based On Loop Gain  $T_A$ . The Bode plots of the plant and EA transfer functions, as well as the Bode plots of loop gain  $T_A$ , are shown in Fig. 10. The EA compensation with  $\omega_i = 1.2 \cdot 10^3 \text{ rad/sec}$ ,  $f_{z1} = f_{z2} = 550 \text{ Hz}$ ,  $f_{p1} = f_{p2} = 10 \text{ kHz}$  was chosen to provide 7.1-kHz  $T_A$  bandwidth with the corresponding phase margin of  $63^\circ$ . As can be seen from Fig. 10, for this EA compensation, loop gain  $T_B$  has only 90-Hz bandwidth and corresponding  $105^\circ$  phase margin. This implies that a wide bandwidth of  $T_A$  does not translate into a wide bandwidth of  $T_B$ .

Error Amplifier Design Based On Loop Gain  $T_B$ . The Bode plots of the plant and EA transfer functions, as well as of the loop gain  $T_B$ , are shown in Fig. 11. The EA compensation with  $\omega_i = 40 \cdot 10^3 \text{ rad/sec}$ ,  $f_{z1} = f_{z2} = 2 \text{ kHz}$ ,  $f_{p1} = 2.6 \text{ kHz}$ , and  $f_{p2} = 40 \text{ kHz}$  was selected to provide 6.9-kHz  $T_B$  bandwidth with the corresponding phase margin of  $58^\circ$ . Figure 11 also shows loop gain  $T_A$  for the EA design mentioned above. Observation of Fig. 11 reveals 7.2-kHz  $T_A$  bandwidth with the phase margin of  $55^\circ$ .

Figure 11 also shows that loop gain  $T_A$  is conditionally stable since its phase drops below  $-180^\circ$  around 1-kHz frequency which is within the bandwidth of  $T_A$ . The conditional stability is more pronounced at high Q values of the power stage transfer function. Generally, the conditional stability is not acceptable since the power supply can become unstable during large-signal line transients or as a result of component degradation. Loop gain  $T_B$  in Fig. 11 does not show the conditional stability problem because the power stage characteristics are hidden within  $T_{INNER}$  bandwidth and  $G_{PL(B)}$  is not proportional to such critical gains of the inner loop, as the input voltage and the optocoupler CTR. Therefore, the EA design based on loop gain  $T_A$  is preferable to the one based on loop gain  $T_B$ .

### B. Power Supply with Current-Mode Control

The parameter values assumed for the current-mode control are  $F_M = 2.86 \text{ V}^{-1}$  and  $R_S = 25 \text{ m}\Omega$ . Figure 12 shows the detailed small-signal block diagram of the converter with the current-mode control. The diagram contains the internal current control loop with following blocks:

$G_{ID} = \hat{i}_L / \hat{d}$  - duty-ratio-to-inductor-current transfer function,  
 $H_E$  - sampling transfer function [12],  
 $R_S$  - current sensing gain,

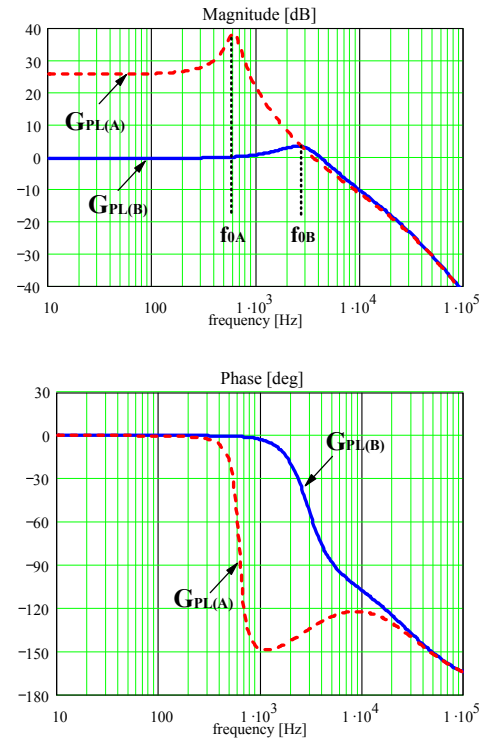


Fig. 9. Transfer functions of plants A and B for voltage-mode control.

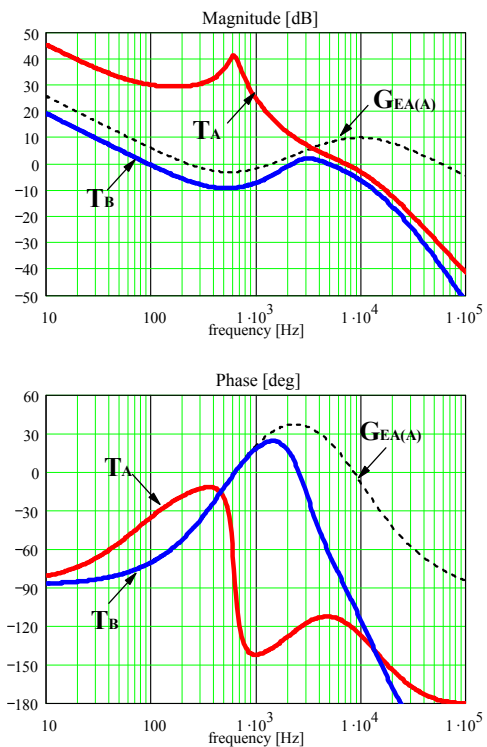


Fig. 10. Loop gain design based on plant A for voltage-mode control.

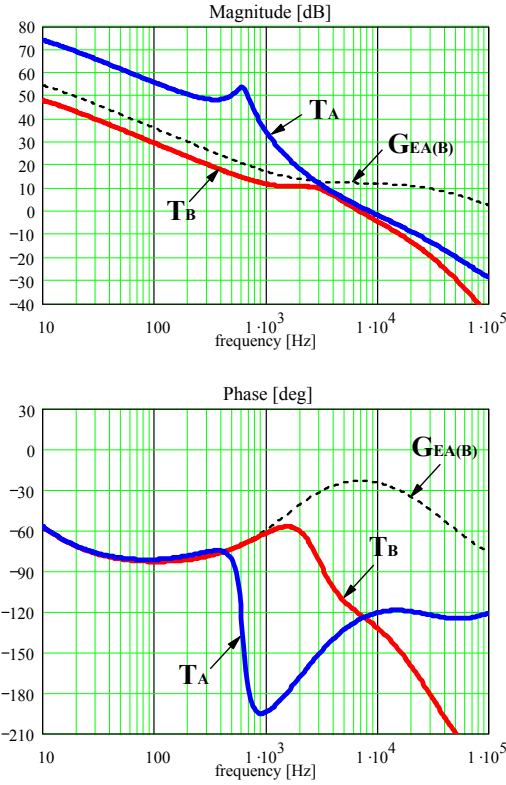


Fig. 11. Loop gain design based on plant B for voltage-mode control.

$F_M$  – PWM gain.

Based on the diagram in Fig. 12, the control-to-output transfer function is described by equation

$$G_{VC} = \frac{F_M \cdot G_{VD}}{1 + F_M \cdot G_{ID} \cdot R_S \cdot H_E} \quad (25)$$

Transfer function  $G_{ID}$  in (25) is derived based on the PWM switch model [13]

$$G_{ID} = \frac{V_{IN}}{N \cdot R_L} \cdot \frac{1 + s/\omega_{ZC2}}{1 + s/(\omega_0 \cdot Q) + s^2/\omega_0^2}, \quad (26)$$

where  $\omega_{ZC2} = 1/(R_C \cdot C_F)$ .

The Bode plots of plant transfer functions  $G_{PL(A)}$  and  $G_{PL(B)}$  are shown in Fig. 13. As Fig. 13 demonstrates, the plant transfer functions are different at low frequencies where  $A_{OC} \cdot G_{VC} \gg 1$ . Actually, due to the inner loop influence, the plant B phase characteristic exhibits less phase lag at low frequencies and, therefore, loop gain  $T_B$  is easier to compensate than loop gain  $T_A$ . The next step is to compare EA designs based on loop gains  $T_A$  and  $T_B$ .

#### Error Amplifier Design Based On Loop Gain $T_A$

Figure 14 shows the loop gain design for plant A which produces following locations of compensator poles and zeroes  $\omega_i = 3.45 \cdot 10^3$  rad/s,  $f_{z1} = 100$  Hz, and  $f_{p1} = 50$  kHz. This design provides 10-kHz loop bandwidth with the corresponding phase margin of 97°. Figure 14 also shows loop gain  $T_B$  corresponding to the compensator design for plant A. The loop gain  $T_B$  has 2.7-kHz loop bandwidth with the corresponding phase margin of 133°.

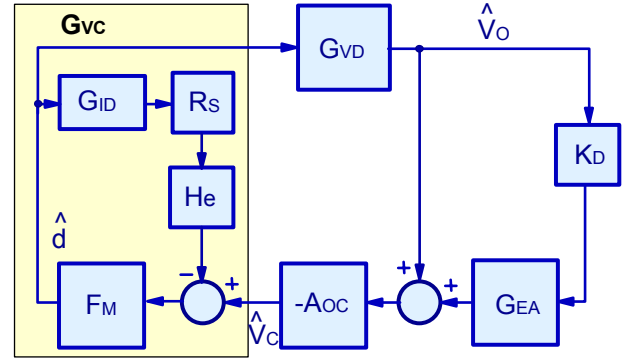


Fig. 12. Small-signal block diagram of isolated power supply with current-mode control.

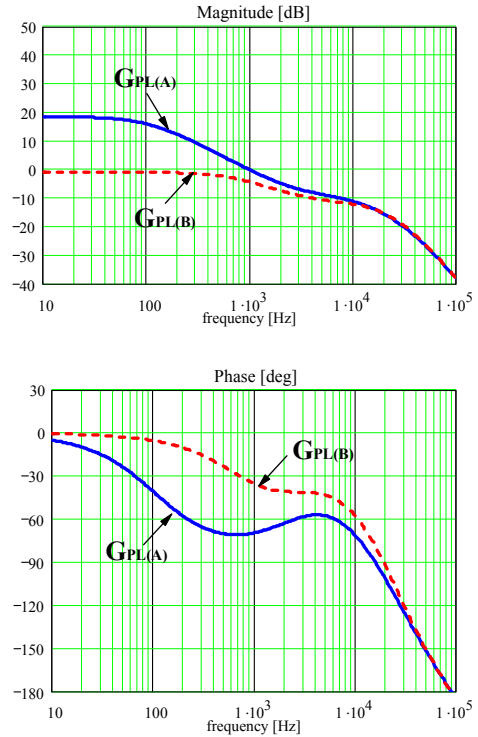


Fig. 13. Transfer functions of plants A and B for current-mode control.

Error Amplifier Design Based On Loop Gain  $T_B$ . The corresponding EA transfer function and loop gain  $T_B$  are plotted in Fig. 15. The compensator has following poles and zeroes:  $\omega_i = 105 \cdot 10^3$  rad/s,  $f_{z1} = 2$  kHz, and  $f_{p1} = 50$  kHz. This design provides 10-kHz loop bandwidth for loop gain  $T_B$ , the same as the bandwidth for loop gain  $T_A$  in the case when the design was done for plant A. The phase margin of loop gain  $T_B$  is 95°. Figure 15 also shows loop gain  $T_A$  corresponding to the compensator design for plant B. The loop gain  $T_A$  has 15-kHz loop bandwidth with the phase margin of 68°.

Observation of Figs. 9-11 and 13-15 implies that the magnitude of loop gain  $T_A$  is higher than that of loop gain  $T_B$ .  $|T_A|$  is higher than  $|T_B|$  at low frequencies since  $|G_{PL(A)}|$  is higher than  $|G_{PL(B)}|$  at low frequencies.  $|T_A|$  is higher than  $|T_B|$  at high

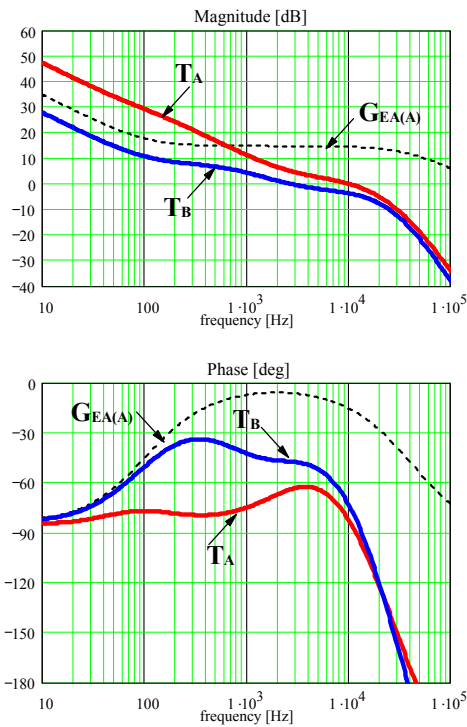


Fig. 14. Loop gain design based on plant A for current-mode control.

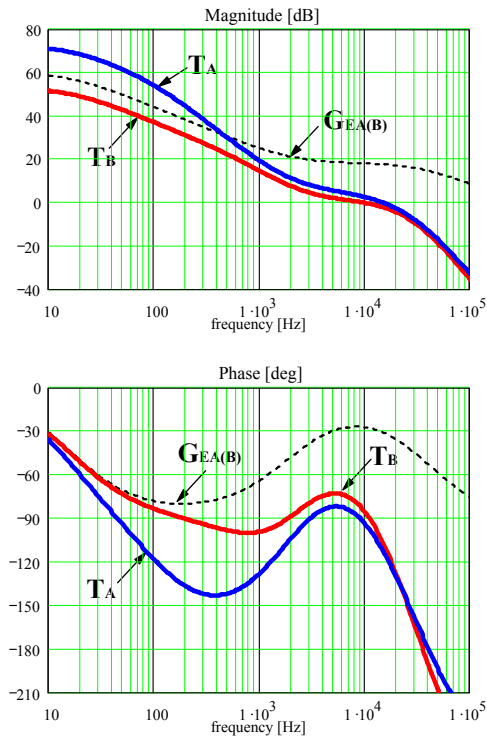


Fig. 15. Loop gain design based on plant B for current-mode control.

frequencies since  $|1+K_D \cdot G_{EA}|$  is higher than  $|K_D \cdot G_{EA}|$  at high frequencies. At the same time, the phase lag of loop gain  $T_A$  is generally higher than that of loop gain  $T_B$ . Therefore, if the EA

design is based on loop gain  $T_A$ , loop gain  $T_B$  is expected to have lower bandwidth and higher stability margins than loop gain  $T_A$ .

The presented design example implies that, in the case of the current-mode control, both loop gains  $T_A$  and  $T_B$  can be used for the EA design.

## V. EXPERIMENTAL RESULTS

The 380-V/12-V, 45-A two-switch forward power supply operating at 100-kHz switching frequency was used as an experimental prototype. The power transformer has  $N = 10:1$  turns ratio. The output filter inductor value was  $L_F = 11.5 \mu\text{H}$ , whereas output capacitance  $C_F$  consisted of three 3300- $\mu\text{F}$  aluminum capacitors with 35-m $\Omega$  ESR each. The converter operated with the current-mode control that was implemented by measuring the primary switch current with the 0.15- $\Omega$  resistor. Compensation network  $Z_2$  was a series connection of 27-k $\Omega$  resistor and 5.6-nF capacitor, whereas network  $Z_1$  was not used. Therefore, EA transfer function had the single pole at the origin and one zero at 1-kHz frequency. The second compensation pole was introduced by the optocoupler network on the primary side. The prototype employs SHF617-3 optocoupler with the CTR range of 100-200 % for  $I_F = 10 \text{ mA}$ . The component values of the optocoupler circuit are  $R_1 = R_2 = 1 \text{ k}\Omega$ ,  $C_2 = 4.7 \text{ nF}$ , where  $C_2$  is the sole component of compensation network  $Z_3$  in Fig. 1.

Bode plots of the transfer functions corresponding to breaking the loop at point A are shown in Fig. 16. As expected

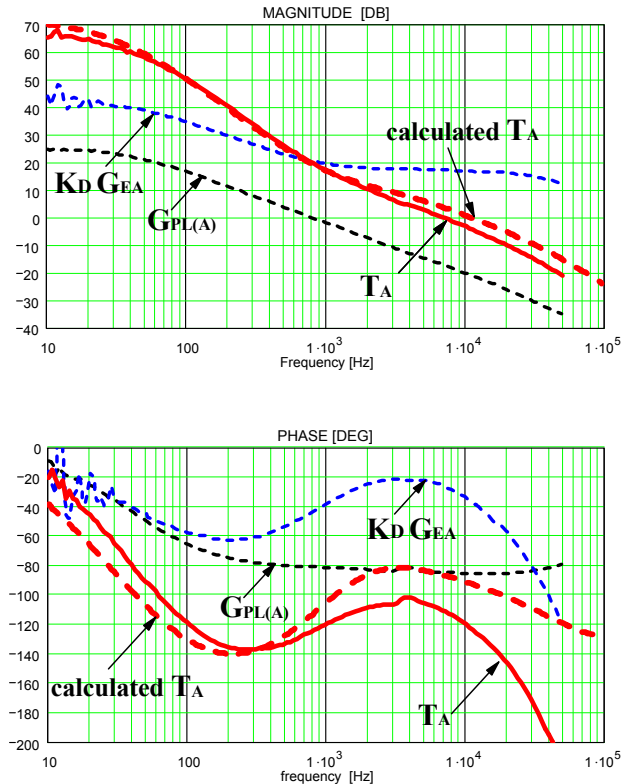


Fig. 16. Measured and calculated transfer functions corresponding to breaking the loop at point A.

## VI. SUMMARY

In the isolated power supplies with the optocoupler feedback, two loops can be identified with corresponding loop gains  $T_A$  and  $T_B$ . The comparative analysis shows that loop gain  $T_A$  provides more straightforward design approach and more meaningful relationship between the loop gain and converter response to the line and load disturbances. It was found that in power supplies with the current-mode control both loop gains can be used for the compensation design. However, in the power supplies with the voltage-mode control the bandwidth can be very different depending on which loop gain was used for the compensator design. Also, in the power supplies with the voltage-mode control it is preferable to use the loop gain  $T_A$  for the EA design in order to avoid the conditional stability. Dynamic limitations of the TL431 shunt regulator and of the optocoupler were discussed. Practical guidelines for the compensation design in converters with current-mode and voltage-mode controls, as well as experimental results were presented.

## REFERENCES

- [1] B. Mammono, "Isolating The Control Loop," *Unitrode Seminar Proc.*, 1997, pp. C2-1 - C2-15.
- [2] K. Billings, "Handbook Of Switchmode Power Supplies", *McGraw-Hill Publishing Company*, 1989.
- [3] D. Venable, "Stability Testing of Multiloop Converters", *Venable Technical Paper # 11*, [www.venable.biz/tr-papers2.html](http://www.venable.biz/tr-papers2.html).
- [4] T. H. Chen, "Dynamic Modeling And Control Design Of Flyback Converter," *IEEE Transactions on Aerospace and Electronic Systems*, Vol. 35, No. 4, pp. 1230-1239, Oct. 1999.
- [5] R. Kollman, J. Betten, "Closing the Loop with a Popular Shunt Regulator," *Power Electronics Technology Magazine*, pp. 30-36, Sept. 2003.
- [6] R. Kollman, J. Betten, "Compensating the (Often Missed) Inner and Outer Control Loops Using the TL431," *Power Electronics Technology Conference Proc.*, Rosemont, Illinois, pp. 366-377, Oct. 2002.
- [7] I. Ozkaynak, "Use of Optocoupler or Current Mirror to Eliminate LC Output Filter Effects in Buck-Boost Topology," *Power Electronics Technology Conference Proc.*, Rosemont, Illinois, pp. 378-388, Oct. 2002.
- [8] C.H. Yang, D.Y. Chen, C. Jamerson, Y.P. Wu, "Stabilizing Magamp Control Loop by Using an Inner-Loop Compensation," *Applied Power Electronics Conference Proc.*, pp. 365-372, March 1991.
- [9] I.J. Lee, D.Y. Chen, C. Jamerson, Y.P. Wu, "Modeling of Control Loop Behavior of Magamp Post Regulators," *Applied Power Electronics Conference Proc.*, pp. 365-372, March 1991.
- [10] R. W. Erickson, D. Maksimovic, "Fundamentals of Power Electronics," Norwell, MA: Kluwer Academic Publishers.
- [11] J. Bliss, "Theory and Characteristics of Phototransistors," *Motorola Application Note AN-440*, *Motorola Databook "Optoelectronics Device Data"*, pp. 9.3 - 9-13.
- [12] R. B. Ridley, "A New, Continuous-Time Model for Current-Mode Control," *Power Conversion and Intelligence Motion Conference Proc.*, Long Beach, CA, pp. 455-464, Oct. 1989.
- [13] V. Vorperian, "Simplified Analysis of PWM Converters Using the Model of the PWM Switch Part I: Continuous Conduction Mode", *VPEC Seminar Proc.*, Blacksburg, VA, September 1989, pp. 1-9.

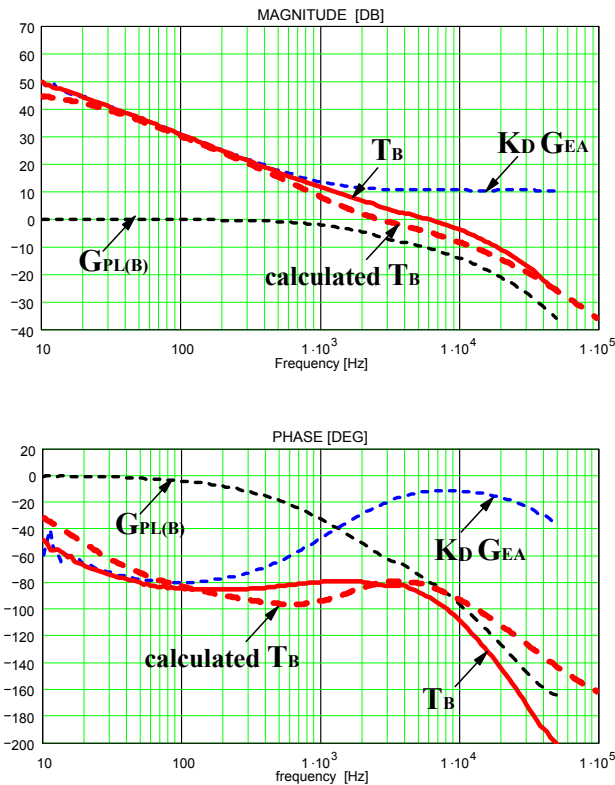


Fig. 17. Measured and calculated transfer functions corresponding to breaking the loop at point B.

for the current-mode control,  $G_{PL(A)}$  is the first-order transfer function with the dominant pole located around 40 Hz. Since  $K_D \cdot G_{EA} \gg 1$  in the frequency range up to half of the switching frequency, the loop gain is

$$T_A \approx G_{PL(A)} \cdot A_{OC} \cdot K_D \cdot G_{EA}$$

and EA design procedure is conventional. Loop gain  $T_A$  has the crossover frequency of 6.7 kHz, the phase margin of  $68^\circ$  and the gain margin of 18 dB.

Figure 17 shows Bode plots of the transfer functions corresponding to breaking the loop at point B. At low frequencies, plant transfer function  $G_{PL(B)}$  is close to 0 dB and its phase is also close to zero. The EA phase is supposed to reach  $0^\circ$  at high frequencies and stay at this value. However, at frequencies above 10 kHz the EA phase starts to drop because of the insufficient TL431 open-loop gain in the high-frequency range. Resulting gain  $T_B$  has the bandwidth of 5.6 kHz, the phase margin of  $90^\circ$  and the gain margin of 19 dB.

Observation of Figs. 16 and 17 implies that loop gains  $T_A$  and  $T_B$  have similar crossover frequencies and stability margins for the optimized compensation and can be both used for the EA design.

For analysis verification, Figs. 16 and 17 also show calculated loop gains  $T_A$  and  $T_B$ . Measured and calculated loop gains demonstrate reasonable agreement with each other.